The Structure of L-Hydantoinase from *Arthobacter aurescens* Leads to an Understanding of Dihydropyrimidinase Substrate and Enantio Specificity[†,‡]

Jan Abendroth,[§,||] Karsten Niefind,[§] Oliver May,[⊥] Martin Siemann,[⊥] Christoph Syldatk,[⊥] and Dietmar Schomburg*[,§]

Institut für Biochemie, Universität zu Köln, Zülpicher Strasse 47, 50674 Köln, Germany, and Institut für Bioverfahrenstechnik, Universität Stuttgart, Allmandring 31, 70569 Stuttgart, Germany

Received September 13, 2001; Revised Manuscript Received April 16, 2002

ABSTRACT: L-Hydantoinase from *Arthrobacter aurescens* (L-Hyd) is a member of the dihydropyrimidinases which in turn belong to the cyclic amidases. Dihydropyrimidinases catalyze the reversible hydrolytic ring opening of dihydropyrimidines as the second step in the catabolism of pyrimidines. In biotechnology, their hydroloytic activity on five-membered cyclic diamides (hydantoins) is used in the enantio-specific production of amino acids from racemic hydantoins. L-Hyd differs from most of the other dihydropyrimidinases by an L-enantio specificity and by lacking activity on possible natural substrates such as dihydropyrimidines. In this paper, we describe the three-dimensional structure of L-Hyd which was solved by molecular replacement using a homology model and subsequently refined to 2.6 Å resolution. Each subunit of the tetrameric L-Hyd consists of an elliptically distorted $(\alpha/\beta)_8$-barrel domain, which hosts the active site, and a β-sheet domain. In the active site, a binuclear zinc center activates a water molecule for nucleophilic attack on the substrates' amide bond. L-Hyd shows a strong homology both in fold and in metal coordination in the active site to another dihydropyrimidinase from *Thermus sp.* (D-hydantoinase) and to a slightly lesser degree to ureases, dihydroorotase and phosphotriesterase. Using the homology to ureases, a model for the transition state was modeled in the active site of L-Hyd and D-hydantoinase. This model could provide an explanation for the different substrate and enantio selectivities of both dihydropyrimidinases.

Hydantoinases. Dihydropyrimidinases (EC 3.5.2.2) belong to the group of cyclic amidases. Because of their biotechnological application, hydantoinase is frequently used as synonym for prokaryotic dihydropyrimidinases. Dihydopyrimidinases catalyze the reversible hydrolytic ring opening of six- or five-membered cyclic diamides such as dihydropyrimidines and 5′-monosubstituted hydantoins to the corresponding 3-ureido acids and carbamoyl amino acids, respectively (Figure 1a,b).

The physiological function of dihydropyrimidinases is the hydrolysis of dihydropyrimidines as the second step in the reductive catabolism of pyrimidines (*1*). Some closely related enzymes (*2, 3*) do not hydrolyze dihydropyrimidines. Their natural function still remains unclear. However, in this paper all these enzymes are called dihydropyrimidinase, as all hydrolyze 5′-monosubstituted hydantoins. Diseases due to disturbed pyrimidine degradation caused by less active or inactive dihydropyrimidinase are scarce, but have been reported for some patients (*4, 5*).

In biotechnology dihydropyrimidinases are used in combination with carbamoylases as biocatalysts for the enantio-

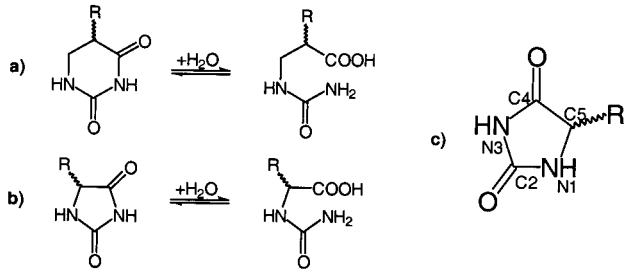

FIGURE 1: Reactions catalyzed by dihydropyrimidinases. Hydrolysis of (a) dihydropyrimidines to 3-ureido acids and (b) 5′-monosubstituted hydantoins to carbamoyl amino acids. (c) Numbering of the atoms in the hydantoin ring.

specific enzymatic production of non-proteinogenic amino acids from racemic hydantoins (*6*). The products are valuable precursors, e.g., for the synthesis of β-lactam antibiotics or synthetic peptides. Due to different enantio selectivities on their biotechnological substrates, dihydropyrimidinases were traditionally divided in L- (*7*), non-, or D-enantio-specific (*8, 9*) hydantoinases.

The biochemical properties and the substrate specificities of a broad set of dihydopyrimidinases have been charaterized mainly from a biotechnological point of view [reviewed by Syldatk et al. (*10*)]. All dihydopyrimidinases are metal-dependent. In most cases, the cofactor is Zn^{2+}, which can be substituted with other divalent transition-group metals such as Mn^{2+} or Co^{2+}. Most of the dihydropyrimidinases form tetramers.

[†] The work of J.A. was supported by the Deutsche Forschungsgemeinschaft.

[‡] The coordinates and structure factors of L-Hyd have been deposited in the Protein DataBank under accession code 1GKR.

* Corresponding author. Email: D.Schomburg@uni-koeln.de.

[§] Universität zu Köln.

[||] Current address: Howard Hughes Medical Institute and Department of Biochemistry, University of Washington, Seattle, WA 98195.

[⊥] Universität Stuttgart.

10.1021/bi0157722 CCC: $22.00
Published on Web 06/17/2002

Different dihydopyrimidinases share more than 30% sequence identity. A close evolutionary relationship between dihydopyrimidinases and other amidohydrolases such as allantoinases (sequence identity 30%), dihydroorotases (>25%), and ureases (20%) was proposed by Holm and Sander (*11*) and May et al. (*12*). There are significant but unexpected homologies with the non-catalytic proteins TOAD (turned on after division) and CRMP (collapsin response mediator protein) which are involved in the development of the nervous system (*13*).

Recently, we reported the structure of a dihydropyrimidinase from *Thermus sp.* (D-hydantoinase, pdb accession number 1GKP) refined to 1.3 Å resolution (*14*). In this structure, each monomer in the homotetramer consists of a central elliptically distorted $(\alpha/\beta)_8$-barrel which hosts the active site, and a β-sheet domain. The fold of D-hydantoinase has a strong homology with the α-subunits of ureases from *Klebsiella aerogenes* (*15*) and from *Bacillus pasteurii* (*16*), with dihydroorotase from *E. coli* (*17*), and with the phosphotriesterase from *Pseudomonas diminuta* (*18*). They share a very similar central $(\alpha/\beta)_8$-barrel whereas the size of the β-sheet domain varies strongly in the different structures.

The activation of the nucleophile for the hydrolytic reaction is highly conserved in all these structures. A water molecule is located between two zinc ions which causes a significant reduction of the pK_a of this water. The metal ions are either zinc (D-hydantoinase, dihydroorotase, and phosphotriesterase) or nickel (urease). The ligands of the metal ions (two histidines each, one aspartate, and one carboxylated lysine which bridges the two zinc ions) are highly conserved. Urease, dihydroorotase, and phosphotriesterase have been crystallized with bound inhibitors and/or substrates which are located in close proximity to the activated water.

The L-hydantoinase from *Arthrobacter aurescens* strain DSM 3745 (L-Hyd) described in this paper was purified and characterized by May et al. (*3, 12, 19, 20*). In contrast to most of the other dihydopyrimidinases, L-Hyd does not hydrolyze dihydropyrimidines. The natural function of L-Hyd is not yet known. Its expression in *Arthrobacter aurescens* is induced by 3-*N*-methyl-5-(3′-indolylmethyl)-hydantoin. In the genome of *Arthrobacter aurescens*, a hydantoin racemase and an L-*N*-carbamoylase are located upstream and downstream of the L-Hyd gene, respectively (*21*).

L-Hyd consists of 458 amino acids and forms tetramers in the native state. It is a zinc-dependent enzyme. Chemical modification of the active site histidines leads to irreversible removal of the zinc with chelating agents to reversible deactivation. The latter can be restored by incubation of the apo-enzyme with Mn^{2+} and Co^{2+}. A total of 2.5 zinc ions per monomer were presumed as assessed by atomic absorption analysis. As the deactivation of the enzyme by removal of zinc also leads to a disassembly of the tetramer to monomers, both catalytic and structural functions were assigned to zinc.

The substrate and enantio specificity of L-Hyd was examined in detail by May et al. (*3*) and Waniek (*22*). L-Hyd is predominantly L-enantio specific and prefers hydantoins with bulky and methylene-bridged aromatic (benzyl) side chains. In contrast, D-hydantionase prefers 5′-phenyl-substituted hydantions with a high D-enantio specificity (*23*). The enantio specificity of L-Hyd is substrate-dependent: For methyl-thioethyl-hydantoin, the D-enantiomer is preferred. Directed evolution of L-hydantoinase from *Arthrobacter aurescens* DSM 9771 led to single-residue mutants with altered enantio specificity (*36*). Hydantoin analogues with the nitrogen on the N1-position of the hydantoin ring (Figure 1) methylated or substituted by oxygen, sulfur, or a methylene group or with the nitrogen on the N3-position substituted by a methylene group are very little or not hydrolyzed (*22*). This underlines that for catalyis a hydrogen bond donor is important on this position.

Phylogenetic examinations (*12*) revealed that L-Hyd has diverged early in the evolution from other hydantoinases. Furthermore, due to its substrate-dependent enantio selectivity which can be altered by single-residue mutations, the traditional classification of hydantoinases based on their enantio selectivity was queried.

MATERIALS AND METHODS

Expression, Purification, Crystallization, and X-ray Measurements. Expression, purification (*3*), crystallization, and X-ray diffraction measurements (*24*) have been described elsewhere by May et al. The crystals belong to space group $P2_1$ with unit cell parameters $a = 111.55$ Å, $b = 74.28$ Å, $c = 146.87$ Å, and $\beta = 106.7°$. An X-ray diffraction data set had been measured with CuKα radiation up to 2.6 Å resolution containing 124.261 observed and 61.763 unique reflections, with $R_{sym} = 9.1\%$ (14.8% for the highest resolution bin), an overall completeness of 86.6% (41.2%), and an $I/[\sigma(I)]$ of 8.5 (2.5) (*24*). The results of the preliminary analysis of the data set were in accordance with one homotetramer with an internal *222*-symmetry in the asymmetric unit.

Molecular Replacement. Initial trials of using the α-chain of urease from *Klebsiella aerogenes* 2KAU (*15*) (22% sequence identity) as search model with X-PLOR (*25*) and REPLACE (*26*) remained unsuccessful. With the availability of the more homologous structure of D-hydantionase (29% sequence identity), the calculations for the molecular replacement were repeated with CNS (*27*). Both native and poly-Ala-D-hydantoinase as monomer or dimer were used as search models; however, they remained unsuccessful as well. In retrospective, it is evident that using a dimer instead of a monomer did not improve the correlation because of distinct differences in the assembly of the tetramers.

Then a rough homology model of L-Hyd was created. For this purpose, first a multiple sequence alignment of L-Hyd with the α-chain of urease from *Klebsiella aerogenes* and D-hydantionase was done with CLUSTALW (*28*). This sequence alignment and the coordinates of a D-hydantoinase monomer were used for the modeling using the semiautomatic mode of MODELLER (version 4) (*29*).

This modeled monomer was used for molecular replacement calculations with CNS (*27*). The cross-rotation function was calculated in the fast direct mode using data between 10 and 4 Å resolution. A Patterson correlation refinement was done prior to the translation function calculations (fastf2f2 target, 15−4 Å) followed by a rigid-body refinement. In the first translation function, the four correct solutions did not separate from the wrong solutions (see Table 1). Therefore, in the calculations for the second

Table 1: Molecular Replacement: Results of the Different Translation Function Searches after Patterson Correlation Refinement[a]

rank in rotation fuction	1st translation cycle, no molecule fixed		2nd translation cycle, one molecule fixed		3rd translation cycle, two molecules fixed		4th translation cycle, three molecules fixed	
	monitor	packing	monitor	packing	monitor	packing	monitor	packing
1	0.088	0.1227*	0.105	0.1472*	0.138	0.2679*	0.164	0.3852*
2	0.064	0.1225	0.130	0.2442**	0.118	0.2703*	0.162	0.3822*
3	0.056	0.1225	0.095	0.2018	0.154	0.3628**	0.149	0.3867*
4	0.053	0.1134	0.102	0.1713	0.133	0.2813	0.149	0.4078
5	0.051	0.1226	0.095	0.1653	0.130	0.2952	0.151	0.4073
6	0.040	0.1224	0.097	0.1863	0.145	0.1863	0.172	0.4815**
7	0.044	0.1226	0.097	0.1901	0.126	0.3338	0.150	0.4090
8	0.044	0.1131	0.093	0.1953	0.126	0.2969	0.149	0.4051
9	0.061	0.1224	0.094	0.1605	0.130	0.2922	0.155	0.4179
10	0.053	0.1157	0.093	0.1964	0.129	0.3107	0.155	0.4129

[a] Since after the first translation search the four correct solutions did not separate from wrong solutions, the calculations were done in four cycles. After each cycle, one solution was selected (marked with **) due to the different score values of CNS and kept fixed during the following cycles (marked with *). With this iterative translation search, the significance of initially weak solutions could be increased significantly. The top 10 solutions of the rotation function are listed.

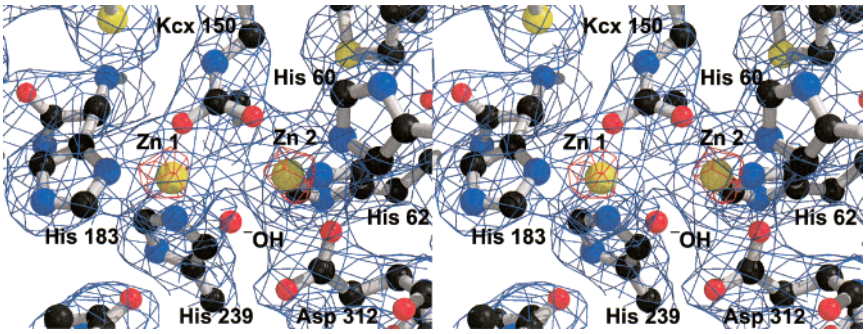

FIGURE 2: Electron density. The final atomic model of the active site of L-Hyd covered by the $2mF_oDF_c$ electron density map contoured at 1σ- (blue) and 8σ-levels (red).

translation function, the top solution of the first translation function was kept fixed, and a second monomer was shifted. With this iterative procedure, the correct solution for the next monomer clearly separated both in scoring and in packing function from the wrong solutions, and the tetramer was assembled step by step. Although the *R*-values after the rigid-body refinement remained comparatively high (R_{work} = 51.6% and R_{free} = 52.3%), the fact that the non-crystallographic symmetry of the tetramer was in accordance with the self-rotation function (*24*) gave evidence that we had chosen the correct orientations.

Model Building and Refinement. Subsequent cycles of model building with O (*30*) were alternated with refinement using the CNS-suite (*27*). In the initial steps, major changes were made during manual model building. Therefore, simulated annealing with torsion angle molecular dynamics was performed prior to maximum likelihood conjugate gradient minimization against native structure factor amplitudes. The NCS symmetry operators were obtained from the initial tetramer and refined further. With regard to the resolution, all subunits of the tetramer were kept absolutely identical throughout the whole refinement by application of constraint NCS symmetry. After the first refinement using data up to 3.0 Å resolution, the *R*-values dropped to R_{work} = 36.9% and R_{free} = 40.3%. Residues with poor density were removed and rebuilt manually. The resolution limit was extended to 2.6 Å, and the protein model was completed. When water was introduced (3σ-level in sigma-weighted F_oF_c map), the *R*-values dropped by 1.4% (R_{work}) and 1.2% (R_{free}), respectively. As a relaxation of the constraint NCS to restraint NCS did not improve the R_{free} significantly, constraint NCS were maintained with respect to the resolution of the diffraction data.

Residues 1−451 could be traced; the remaining 7 C-terminal residues were disordered. The most flexible parts of the structure are several loops, e.g., the long loop between strands β5 and β6. However, all parts of the model could be traced unambiguously. Although there is little electron density between the strong electron density of the zinc atoms (see Figure 2), the homology to other amidases and the limited resolution of the diffraction data justified the introduction of the catalytically important water.

The refinement converged at *R*-values of R_{work} = 23.3% and R_{free} = 25.5%. Statistics on the final model are summarized in Table 2. The stereochemisty of the final model was good; 89.1% of the residues were located in the most favored regions, and 10.2% of the residues were located in the additionally allowed regions of the Ramachandran plot [PROCHECK (*31*)]. Ile 64 is the only residue in the disallowed region of the Ramachandran plot. It is located close to the active site and has a well-defined electron density. Two other residues are located in generously allowed regions: Lys 436 lies in a sharp bend; His 239 is the ligand for one of the active site zincs.

Analysis of the Model and Modeling of Substrates. The quality of the models was assessed continuously during the refinement process with PROCHECK (*31*). The secondary structure elements were assigned with DSSP (*32*). Structures of the transition-state analogues were obtained from CORINA (*33*). The modeling of the transition-state analogues was done manually with the graphic program O (*30*).

Table 2: Quality of the Refined Model and Statistics on the Refinement[a]

contents of model	
protein (residues/atoms)	451/3416
zinc	2
water	131
refinement	
resolution (Å)	30−2.60
R_{work} (%)	22.4
R_{free} (%)	24.3
rmsd from ideality	
bonds (Å)	0.009
angles (deg)	1.66
dihedrals (deg)	24.8
improper (Å^3)	1.12
average *B* factors	
all protein atoms (Å^2)	22.6
main chain atoms (Å^2)	21.1
side chain atoms (Å^2)	24.5
zinc (Å^2)	17.4
waters (Å^2)	30.2
overall (Å^2)	22.9

[a] As the model was refined with constraint NCS, the contents of the model refer to one monomer.

RESULTS AND DISCUSSION

Structure Solution. The structure of L-Hyd was solved by molecular replacement using an X-ray diffraction dataset up to 2.6 Å resolution (*24*). During the calculation for the molecular replacement, the use of a crude homology model of a L-Hyd monomer as search model appeared to be the key step.

Overall Structure. The topology and the overall structure of both L-Hyd monomer and L-Hyd tetramer are illustrated in Figure 3. The monomer measures 70 Å × 50 Å × 50 Å, the tetramer 120 Å × 80 Å × 80 Å. The monomer consists of two domains. A central $(\alpha/\beta)_8$-barrel is flanked by a β-sheet domain, which comprises both the N- and the C-terminus.

The $(\alpha/\beta)_8$-barrel is elliptically distorted. It is built up by strands $\beta8-\beta15$ and helices $\alpha2-\beta5$, $\alpha8-\alpha9$, $\alpha14$, and $\alpha18$, and ranges from residues 56 to 348. It is extended by four α-helices, six short 3_{10}-helices, and a small β-strand. The β-sheet domain consists of two mixed parallel/antiparallel β-sheets. The larger β-sheet is built up by seven strands ($\beta3$, $\beta2$, $\beta7$, $\beta17$, $\beta20-\beta22$), three of them from the N-terminus, the other three from the C-terminus. The smaller β-sheet consists of four strands from the N-terminus ($\beta5$, $\beta4$, $\beta1$, $\beta6$). It is continued in the adjacent monomer.

The comparison of the topologies of L-Hyd and D-hydantoinase (Figure 3c/d) illustrates the strong structural homology between these two enzymes. Smaller differences in the secondary structure elements are instead a result of the secondary structure assignment than real structural differences. More than 45% of the Cα-atoms of L-Hyd can be matched with structurally equivalent Cα-atoms of D-hydantoinase with RMSD = 1.0 Å (cutoff = 1.8 Å). The close structural relationship between dihydopyrimidinases, ureases from *Klebsiella aerogenes* and *Bacillus pasteurii*, phosphotriesterase, and dihydroorotase has been discussed in more detail for D-hydantoinase (*14*). They all share the same elliptically distorted $(\alpha/\beta)_8$-barrel. However, the size of the β-sheet-rich domain varies strongly in these enzymes: In ureases, this domain in significantly larger than in L-Hyd and D-hydantoinase. In dihydroorotase, it only consists of two β-strands; in phosphotriesterase, this domain is missing completely.

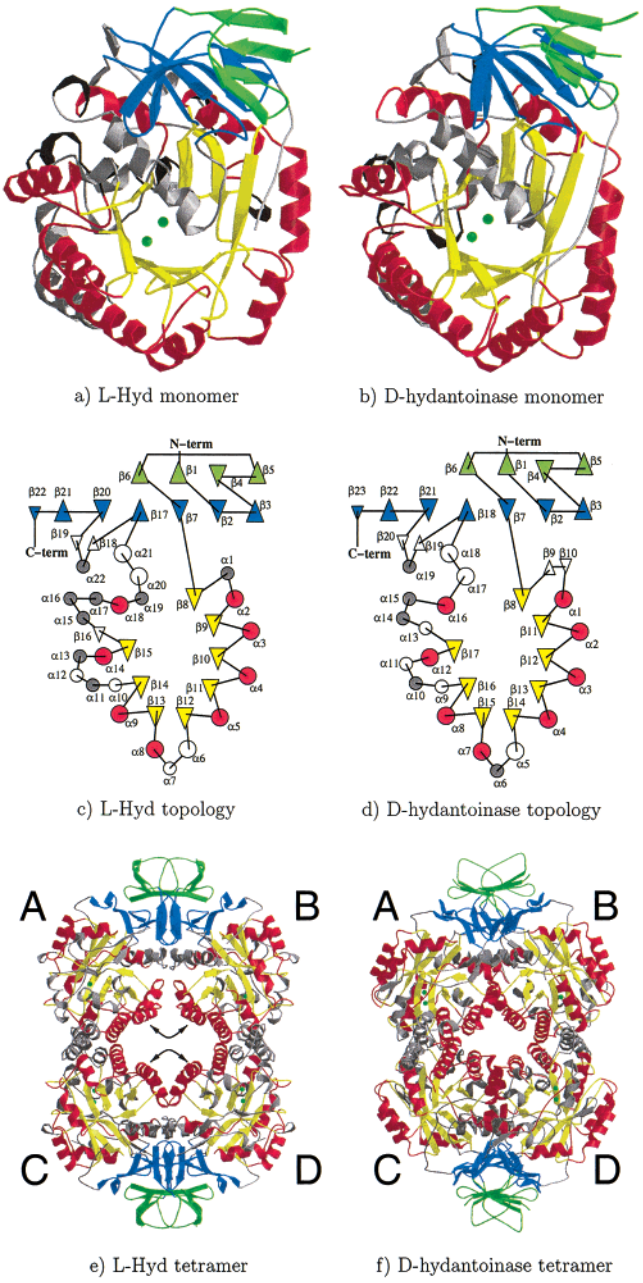

FIGURE 3: Tertiary and quaternary structures. (a, b) Ribbon diagrams of L-Hyd and D-hydantoinase monomers. The central (α/β)-barrels are colored in red and yellow; the two β-sheets are colored blue and green, respectively. (c, d) Topologies of L-Hyd and D-hydantoinase in the same color scheme as in (a, b). β-Strands are represented as triangles pointing in the direction of the strand; α-helices are represented as circles which are colored gray for 3_{10}-helices. (e, f) Ribbon model of L-Hyd and D-hydantoinase tetramers. The opening of the L-Hyd tetramer toward the center of the tetramer is indicated. Created with MOLSCRIPT (*37*) and RASTER3D (*38*); (b) and (d) modified from TOPS (*39*).

Enzymes acting on different enantiomers of a substrate often possess completely different structures. Well-known examples are D- and L-lactate dehydrogenase or D- and L-amino acid oxidases. Against this background, it is quite remarkable that L-Hyd and D-hydantoinase show a strong structural homology. However, one might keep in mind that the natural substrate of L-Hyd is not yet known and

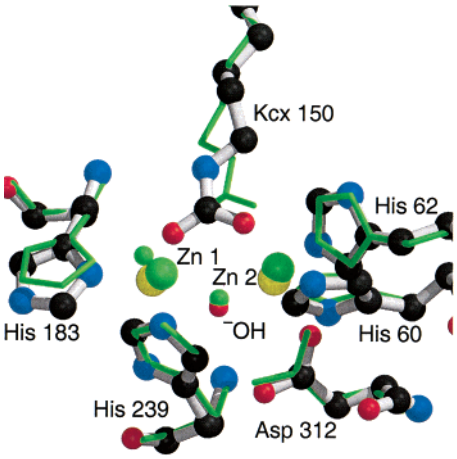

FIGURE 4: Active sites of L-Hyd and D-hydantoinase. Alignment of the active sites of L-Hyd and D-hydantoinase showing the coordination of the active site zincs. The residues of L-Hyd are represented as a ball-and-stick-model, the residues of D-hydantoinase as thin sticks in green. Created with MOLSCRIPT (*37*) and RASTER3D (*38*).

dihydropyrimidines, which are thought to be the natural substrates of D-hydantoinase, have no stereo center.

Quaternary Structure. L-Hyd forms tetramers both in the crystal state (Figure 3e/f) and in solution. The tetramers possess a *222* point group symmetry which is in accordance with the peak pattern of the self-rotation function (*24*). There are two different types of interfaces within the tetramer (Figure 3e): The larger interface is located between subunit A/C or B/D, respectively, and buries 1674 Å^2; the smaller interface is located between subunit A/B or C/D, respectively, and buries 1274 Å^2, compared with the 16 400 Å^2 solvent-accessible surface of one monomer. There is no interface between A/C or B/D, respectively The larger interface is formed by residues from the long helices α5, α6, and α8. The contacts are mediated by both hydrogen bonds and hydrophobic interactions. The smaller interface is mainly formed by residues from strand β5, which continues the small sheet in the adjacent monomer, by residues located in the long loop between strands β5 and β6, and by residues from helix α9. All these contacts are mediated by hydrogen bonds.

Despite the high similarity in the tertiary structures, the tetramers of L-Hyd and D-hydantoinase differ significantly. The dimers A/B and C/D in L-Hyd are more opened toward the center of the tetramer compared with the corresponding subunits in D-hydantoinase, as illustrated in Figure 3e/f. Consequently, the interface between subunits A/B or C/D, respectively, is much smaller in L-Hyd (1274 Å^2) than in D-hydantoinase (2390 Å^2), whereas the interfaces between subunits A/C or B/C, respectively, have a comparable size (1674 Å^2 in L-Hyd vs 1710 Å^2 in D-hydantoinase).

For L-Hyd, it has been reported (*19*) that the deactivation of the enzyme by removal of zinc is accompanied by a disassembly of the tetramers to monomers (*20*). Atom absorption spectroscopy revealed a content of 10 zinc ions in the tetramer (*19*). Therefore, both catalytic and structural function was assigned to zinc. However, no further zinc ions could be detected in the electron density. For various proteins, the assembly to oligmers has a distinct biological function such as allosteric regulation or cooperativity. None of these phenomena has been reported for hydantoinases.

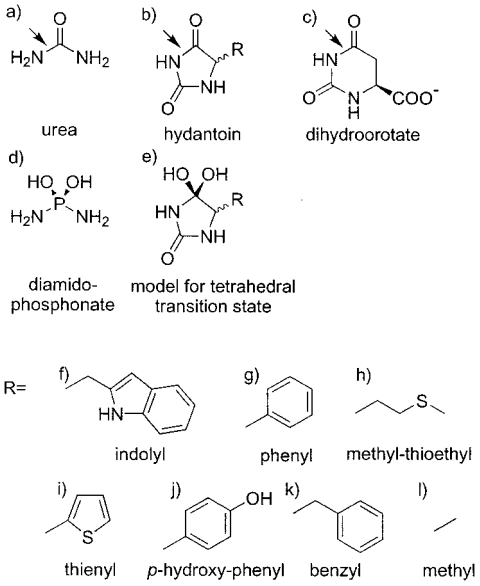

FIGURE 5: Substrates and inhibitors of urease, hydantoinase, and dihydroorotase. Urea, hydantoin, dihydroorotate, and diamidophosphonate as transition-state analogues for urea, model for the tetrahedral transition state of hydantoin and dihydroorotate, and the side chains for the different substrates of L-Hyd and D-hydantoinase discussed in the text.

Active Site. The active site is located at one side of the barrel distant from the β-rich domain at the end of a roughly 15 Å deep hydrophobic cleft. The residues which belong to the active site are in the C-terminal part of different stands of the barrel (β8, β11, β12, β13, β15). The C-terminal part of the strands is the most preferred location of the active site residues in $(\alpha/\beta)_8$-barrel enzymes.

The coordination of the binuclear zinc center and the activation of the nucleophile for the hydrolytic reaction strongly resemble D-hydantoinase, ureases from *Klebsiella aerogenes* and *Bacillus pasteurii*, dihydroorotase, and phosphotriesterase (Figure 4). The structural similarity between the active site of D-hydantoinase, ureases from *Bacillus pasteurii* and *Klebsiella aerogenes*, dihydroorotase, and phosphotriesterase has been described in more detail in a previous report (*14*).

Lysine Kcx 147 of L-Hyd is carboxylated. The same posttranslational modification is also found in the other related enzymes. The two catalytic zinc atoms in the active site are separated by 3.8 Å. Zn 1 is coordinated by Kcx 147 Oδ1, His 183 Nδ, His 239 Nϵ, and ⁻OH 1 O. Zn 2 is coordinated by Kcx 147 Oδ2, His 60 Nϵ, His 62 Nϵ, ⁻OH 1 O, and Asp 312 Oδ1.

The two zinc ions of the active site are bridged by the carbamyl group of Kcx 147 and a hydroxide ion, ⁻OH 1. The close proximity of this water to the two zinc ions lowers its pK_a. This enables it to perform the nucleophilic attack on the carbonyl carbon of the scissile amide bond of the hydantoin ring. The restricted resolution of the data set of L-Hyd (2.6 Å) did not permit the detection of all the water molecules in the first coordination sphere of the active site residues as in D-hydantoinase (1.3 Å resolution).

Ligand Binding and Catalysis. After solving the native structures of L-Hyd and D-hydantoinase, the structural reasons for the different substrate- and enantio-specificities should be examined. However, attempts of co-crystallizing

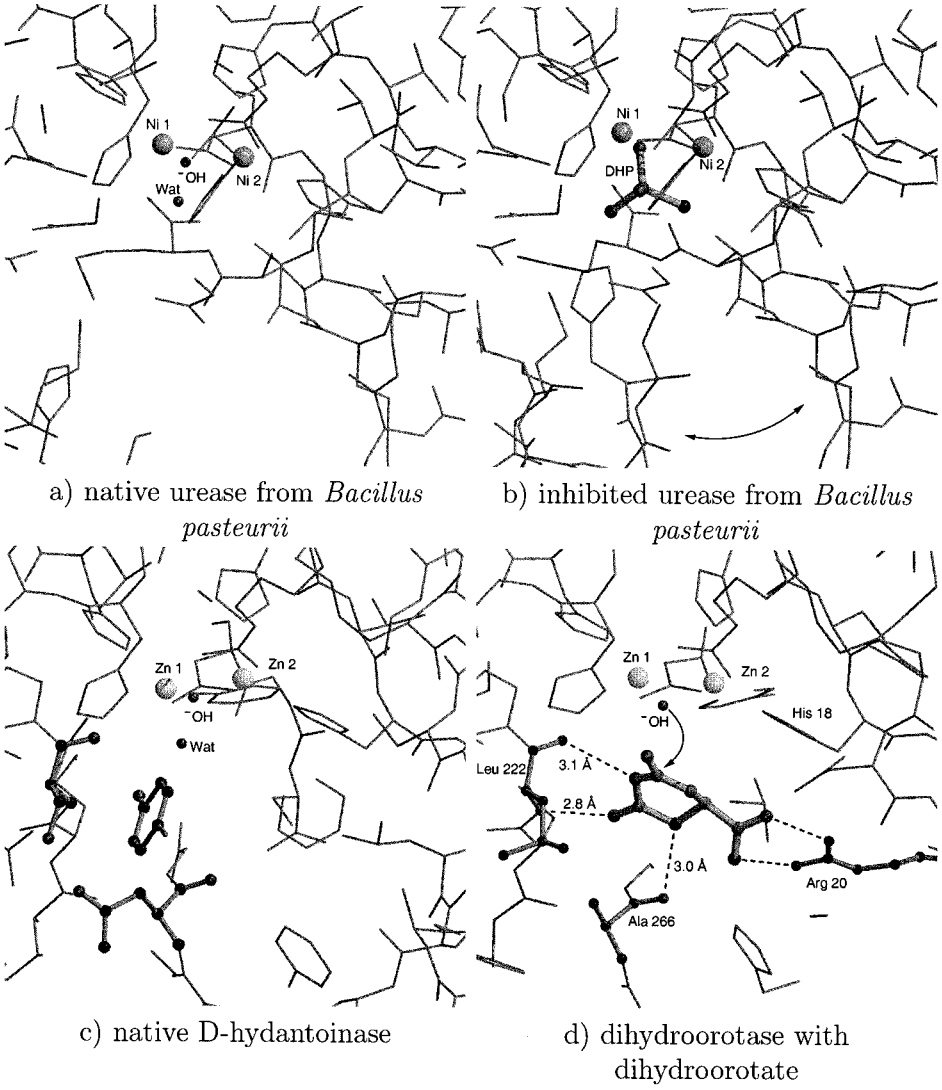

a) native urease from *Bacillus pasteurii*

b) inhibited urease from *Bacillus pasteurii*

c) native D-hydantoinase

d) dihydroorotase with dihydroorotate

a binary complex of protein with substrate failed so far, and potent inhibitors are not known to date. Therefore, the strong structural homology between the active sites of D-hydantoinase, L-Hyd, and structurally related enzymes was exploited for deriving a model for substrate binding.

Urease from *Bacillus pasteurii* has been crystallized (*16*) both as native enzyme and with diamidophosphonate (Figure 5d), which is an analogue for the tetrahedral transition state of urea. The nitrogen or oxygen atoms of diamidophosphonate occupy positions of water molecules in the native structure. The two oxygen atoms of diamidophosphonate replace those two water molecules which are directly bound to the nickel ions. One of these waters is the putative hydroxide ion which is the active nucleophile in the hydrolytic reaction (Figure 6a,b). The two water molecules which are directly bound to the zinc ions could be located in D-hydantoinase on equivalent positions, too [Figure 6c, (*14*)]. The structural conservation of these two water molecules in the active site implies a functional conservation. As a simple model for the tetrahedral transition state in the hydrolysis of the hydantoin ring, the corresponding 4,4′-geminal diols were calculated (Figure 5e). During manual ligand modeling, the two oxygen atoms of the geminal diols were put on the positions of the two structurally conserved water molecules. The orientation of the substrate was then manually optimized by rotation around the axis between these two anchors.

In L-Hyd, the water molecules are much worse defined because of the limited resolution of the diffraction data set as compared to D-hydantoinase. Therefore, the transition-state analogues were first modeled in D-hydantoinase. Their orientation was then transferred to L-Hyd. To minimize the effects of side chain conformation, only those hydantoins were chosen as model substrates which have a minimum number of possible torsion angles and which are hydrolyzed with a high enantio specificity and a high or very low activity.

The proposed orientations of transition-state models of 5′-D/L-indolyl-hydantoin (Figure 5f) in L-Hyd and 5′-D/L-phenyl-hydantoin (Figure 5g) in D-hydantoinase are illustrated in Figure 6e,f. In both enzymes, the hydantoin ring is bound via a comparable hydrogen bond network. There are tight interactions between N3 and O2 of the hydantoin ring and the backbone heteroatoms of Ala 285 in L-Hyd and Ser 288 in D-hydantoinase, respectively. The distance between N1 of the hydantoin ring and the backbone oxygen atoms of Asn 333 (L-Hyd) or Asn 336 (D-hydantoinase), respectively, is beyond the distance of proper hydrogen bonds. However, the importance of a hydrogen bond donor on the N1 position for catalysis could be demonstrated with

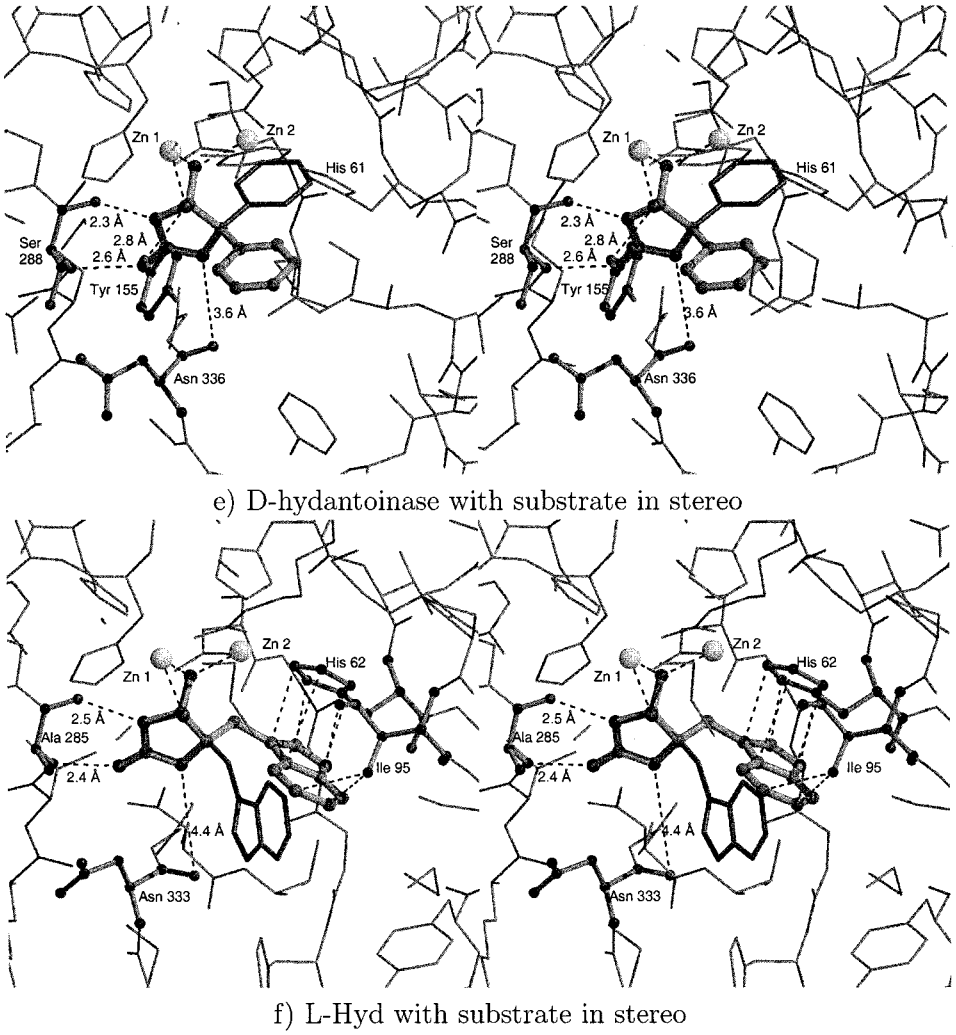

FIGURE 6: Substrate binding and docking. Active sites of (a) native urease from *Bacillus pasteurii* with the active components highlighted; (b) diamidophosphonate-inhibited urease from *Bacillus pasteurii* with the closure of the flexible flap marked with the arrow; (c) native D-hydantoinase; (d) dihydroorotase with bound dihydroorotate and with the residues involved in substrate binding highlighted and the nucleophilic attack of the hydroxide ion indicated with the arrow; (e) D-hydantoinase with D- and L-5′-phenyl-hydantoin in the proposed orientation as ball-and-stick and stick models, respectively. The putative hydrogen bonds are indicated. (f) L-Hyd with L- and D-5′-indolylmethyl-hydantoin in the proposed orientation as ball-and-stick and stick models, respectively. The putative hydrogen bonds and hydrophobic interactions are indicated. Created with MOLSCRIPT (*37*) and RASTER3D (*38*).

hydantoins derivatives which have substitutions on the N1 position (*22*).

In the recently published structure of dihydroorotase (*17*), both substrate and product are bound to the active site of one monomer each. The orientations of these substrates confirmed a posteriori that the proposed orientation which was derived from the symmetrical urea is also true for asymmetrical *cyclic* diamides (Figure 6d). Interestingly, the binding partners of the corresponding hydrogen bonds of the diamide ring are also backbone atoms of the protein. Tyr 155, which further stabilizes the tetrahedral transition state, is unique for D-hydantoinase and has no equivalents in the other related structures.

Before we discuss the interactions of the side chains of the different substrates with the enzymes, the knowledge about the enzymes' substrate and enantio specificities as determined by May et al. (*3*) for L-Hyd and by Keil et al. (*23*) for D-hydantoinase shall be summarized (compare Table 3): L-Hyd prefers 5′-benzyl-substituted hydantoins such as 5′-indolyl-hydantoin (Figure 5f) which is hydrolyzed with a rather high activity and a high enantio-specificity. Hydantoins with phenyl side chains such as 5′-phenyl-hydantoin (Figure 5g) are hydrolyzed at a very low rate. 5′-Methyl-thioethyl-hydantoin (Figure 5h) is a rather good substrate; however, the D-enantiomer is preferred. D-Hydantoinase prefers 5′-phenyl-substituted hydantoins such as 5′-phenyl-hydantoin (Figure 5g) and 5′-(2-thienyl)-hydantoin (Figure 5i). They are hydrolyzed with a high activity and enantio specificity. Phenylic-substituted hydantoins with a polar group in the aromate such as 5′-(*p*-hydroxyphenyl)-hydantoin (Figure 5j) and benzyl-substituted hydantoins such as 5′-benzyl-hydantoin (Figure 5k) are hydrolyzed with a high enantio specificity but a significantly reduced activity, whereas hydantions with small aliphatic side chains such as 5′-methyl-hydanoin (Figure 5l) are hydrolyzed with a high activity but hardly any enantio-selectivity.

With the models of the transition state in the proposed orientation (Figure 6e,f), these specificities can be explained as follows: In the proposed model, the aromatic rings of D-hydantionase's best substrates (e.g., D-5′-phenyl-hydantoins, Figure 5g) smoothly fit in a pronounced hydrophobic pocket made by Leu 64, Cys 95, Phe 152, Tyr 155, and Phe

Table 3: Activities and Enantio Specificities of L-Hyd (*3*) and D-Hydantoinase (*23*) on Selected Substrates[a]

L-Hyd

substate	activity L (units/mg)	activity D (units/mg)	activity D/L (units/mg)
5-indolyl-hydantoin	70	0.1	nd
5-phenyl-hydantoin	nd	nd	0.3
5-methyl-thioethyl-hydantoin	12	37	nd

D-Hydantoinase

substate	activity (units/mg)	ee (%)	at conversion (%)
5-phenyl-hydantoin	1221	>99	90
5-(2-thienyl)-hydantoin	1351	96	50
5-(*p*-hydroxyphenyl)-hydantoin	52	78	>99
5-benzyl-hydantoin	5	>99	12
5-methyl-hydantoin	759	34	73

[a] For L-Hyd, the enantio specificity is expressed as the enzyme's activity on the individual enantiomers. For D-hydantoinase, the enantio specificity is expressed in enantiomeric excess (ee) when the reaction has reached equilibrium. The amount of substrate converted at the equilibrium state is indicated also.

159. The aromatic ring of the L-enantionmer would lead to steric clashes with His 61 and therefore cannot bind in an orientation which promotes catalysis. This hydrophobic pocket governs the specificities of D-hydantoinase. The dual function of Tyr 155 is remarkable, as it is both part of the hydrophobic pocket and stabilizes the transition state with its hydroxyl group. The aromatic rings of D-5′-benzyl-hydantoins (Figure 5k) do not reach the hydrophobic pocket, whereas the polar hydroxyl group of D-5′-(*p*-hydroxyl-phenyl)-hydantoin makes unfavorable interactions with the hydrophobic pocket. Consequently, the specific activity of D-hydantoinase on these substrates is strongly reduced. The enantio-specificity of D-hydantoinase for substrates with a short side chain (e.g., D/L-5′-methyl-hydantoin, Figure 5l) is low as their side chains are too short for steric conflicts with His 61.

L-Hyd does not hydrolyze dihydropyrimidines; its natural substrate is not yet known. The activity of L-Hyd on biotechnologically interesting substrates is smaller compared to D-hydantoinase, and the active site offers much more space. This might indicate that the natural substrate will differ significantly from hydantoins or dihydropyrimidines. No pronounced hydrophobic pocket guides the substrates, which complicates the explanation for the specificities. The proposed orientation of one of L-Hyd's best known substrates, D/L-5′-indolyl-hydantoin (Figure 5f), is illustrated in Figure 6f. Whereas the indole ring of the D-enantiomer would not find any hydrophobic interaction partners, the indole ring of the preferred L-enantiomer can make hydrophobic interactions with the side chains of His 62 and Ile 95. The dual role of His 62, which makes hydrophobic interactions with the substrate and binds Zn 2, is remarkable. The side chains of phenyl-hydantoins such as L-5′-phenyl-hydantoin (Figure 5g) clash with His 62 and are very poor substrates. Therefore, the methlyene bridge of the preferred benzyl-hydantoins is vital for hydrolysis.

5′-Methyl-thioethyl-hydantoin (Figure 5h) is the precursor in the production of methinoine and is an example of a substrate with a long and flexible side chain. The enantio specificity of L-Hyd on 5-methyl-thioethyl-hydantoin has been modified with single-point mutations obtained by directed evolution (*36*). It is difficult to model the flexible side chain. However, one can anticipate the following effects of these mutations: The V154A mutation increases the D-enantio specificity as it offers more space for the side chain of D-5-methyl-thioethyl-hydantoin. The I95F mutation increases the L-enantio specificity as it increases the hydrophobicity close to the side chain of L-5-methyl-thioethyl-hydantoin.

L-Hyd does not hydrolyze dihydropyrimidines and has separated in an early state in the evolution from other dihydopyrimidinases (*12*). In this paper, L-Hyd is considered as a dihydopyrimidinases because of its high structrual homology to D-hydantoinase. Apart from an explanation for the enantio and substrate specificities, we had hoped that the structure of L-Hyd might give hints for potential natural substrates and the enzyme's natural function. However, the large and little pronounced binding pocket makes a prediction difficult.

Currently, two different reaction mechanisms are discussed for ureases (*34*, *16*, *35*) or dihydroorotase (*17*). In the traditional reaction mechanism, the two nickel atoms have different functions: Ni 1 activates the nucleophile, whereas Ni 2 binds the substrate which leads to a tetrahedral transition state with each of the two oxygens bound to one nickel. In the novel reaction mechanism (*16*), both nickel atoms activate the nucleophile. Ni 1 binds the carbonyl oxygen and polarizes the carbonyl bond. Ni 2 binds the amide nitrogen distant to the scissile amide bond. The reaction mechanism proposed for dihydroorotase (*17*) is similar to the novel mechanism for ureases. Zn 1 (β-Zn in the dihydroorotase nomenclature) has the same function as Ni 1 in urease. Zn 2 (α-Zn) only activates the bridging water and does not bind the substrate as in dihydroorotate there is no nitrogen on the corresponding position. In all cases, Asp bound to metal 2 is responsible for protonation and deprotonation. The reaction mechanism proposed for dihydroorotase seems to be applicable for dihydopyrimidinases, too.

The model for substrate binding of L-Hyd and D-hydantoinase derived by homology to ureases provides an explanation for the enzymes' enantio- and substrate-specificities and is consistent with several experimental findings. Although it is further supported by the structure of dihydroorotase, it remains a model until the co-crystallization of the enzymes with substrates of tight binding inhibitors which are not yet available.

REFERENCES

1. Vogels, G. D., and van der Drift, C. (1976) Degradation of purines and pyrimidines by microorganisms. *Bacteriol. Rev. 40*, 403−468.
2. Runser, S. M., and Meyer, P. C. (1993) Purification and biochemical characterisation of the hydantoin hydrolyzing enzyme from *Agrobacterium* species. A hydantoinase with no 5,6-dihydropyrimidine amidohydrolase activity. *Eur. J. Biochem. 213*, 1315−1324.
3. May, O., Siemann, M., Pietzsch, M., Kiess, M., Mattes, R., and Syldatk, C. (1998) Substrate-dependent enantioselectivity of a novel hydantoinase from *Arthrobacter aurescens* DSM 3745: purification and characterisation as new member of cyclic amidases. *J. Biotechnol. 61*, 1−13.
4. van Gennip, A. H., Abeling, N. G., Vreken, P., and van Kuilenburg, A. B. (1997) Inborn errors of pyrimidine degradation: clinical, biochemical and molecular aspects. *J. Inherit. Metab. Dis. 20*, 203−213.

5. Hamajima, N., Kouwaki, M., Vreken, P., Matsuda, K., Sumi, S., Imaeda, M., Ohba, S., Kidouchi, K., Nonaka, M., Sasaki, M., Tamaki, N., Endo, Y., De Abreu, R., Rotteveel, J., van Kuilenburg, A., van Gennip, A., Togari, H., and Wada, Y. (1998) Dihydropyrimidinase deficiency: structural organization, chromosomal localization, and mutation analysis of the human dihydropyrimidinase gene. *Am. J. Hum. Genet. 63*, 717−726.
6. Pietzsch, M., and Syldatk, C. (1995) Hydrolysis and formation of hydantoins. in *Enzyme catalysis in organic chemistry* (Drautz, K., and Waldmann, H., Eds.) pp 409−431, Verlag Chemie, Weinheim, Germany.
7. Yamashiro, A., Yokozeki, K., Kano, H., and Kubota, K. (1988) Enzymatic production of L-amino acids from the corresponding 5′-substituted hydantoins by a newly isolated bacterium *Bacillus brevis* AJ-12299. *Agric. Biol. Chem. 52*, 2851−2856.
8. Möller, A., Syldatk, C., Schulze, M., and Wagner, F. (1988) Stereo- and substrate-specificity of a D-hydantoinase and a D-N-carbamyl-amino acid amidohydrolase from *Arthrobacter crytallopoietes* AM 2. *Enzyme Microb. Technol. 10*, 618−625.
9. Yokozeki, K., and Kubota, K. (1987) Mechanism of asymmetric production of D-amino acids from the corresponding hydantoins by *Pseudomonas sp*. *Agric. Biol. Chem. 52*, 721−728.
10. Syldatk, C., May, O., Altenbuchner, J., Mattes, R., and Siemann, M. (1999) Microbial hydantoinases−industrial enzymes from the origin of life? *Appl. Microbiol. Biotechnol. 51*, 293−309.
11. Holm, L., and Sander, C. (1997) An evolutionary treasure: Unification of a broad set of amidohydrolases related to urease. *Proteins: Struct., Funct., Genet. 28*, 72−82.
12. May, O., Habenicht, A., Mattes, R., Syldatk, C., and Siemann, M. (1998) Molecular evolution of hydantoinases. *Biol. Chem. 379*, 743−747.
13. Hamajima, N., Matsuda, K., Sakata, S., Tamaki, N., Sasaki, M., and Nonaka, M. (1996) A novel gene family defined by human dihydropyrimidinase and three related proteins with differential tissue distribution. *Gene 180*, 157−163.
14. Abendroth, J., Niefind, K., and Schomburg D. (2002) X-ray structure of a dihydropyrimidinase from *Thermus sp.* at 1.3 Å resolution. *J. Mol. Biol.* (in press).
15. Jabri, E., Carr, M. B., Hausinger, R. P., and Karplus, P. A. (1995) The crystal structure of urease from *Klebsiella aerogenes. Science 268*, 998−1004.
16. Benini, S., Rypniewski, W. R., Wilson, K. S., Miletti, S., Ciurli, S., and Mangani, S. (1999) A new proposal for urease mechanism based on the crystal structures of the native and inhibited enzyme from *Bacillus pasteurii*: why urea hydrolysis costs two nickels. *Structure 7*, 205−216.
17. Thoden J. B., Neal, T. M., Raushel, F. M., and Holden, H. M. (2001) Molecular structure of dihydroorotase: a paradigm for catalysis through the use of a binuclear metal center. *Biochemistry 40*, 6989−6997.
18. Vanhooke, J. L., Benning, M. M., Raushel, F. M., and Holden, H. M. (1996) Three-dimensional structure of the zinc-containing phosphotriesterase with the bound substrate analogue diethyl 4-methylbenzylphosphonate. *Biochemistry 35*, 6020−6025.
19. May, O., Siemann, M., Siemann, M. G., and Syldatk, C. (1998) The hydantoin amidohydrolase from *Arthrobacter aurescens* DSM 3745 is a zinc metalloenzyme. *J. Mol. Catal. B: Enzym. 5*, 367−370.
20. May, O., Siemann, M., Siemann, M. G., and Syldatk, C. (1998) Catalytic and structural function of zinc for the hydantoinase from *Arthrobacter aurescens* DSM 3745. *J. Mol. Catal. B: Enzym. 4*, 211−218.
21. Wiese, A., Pietzsch, M., Syldatk, C., Mattes, R., and Altenbuchner, J. (2000) Hydantoin racemase from *Arthrobacter aurescens* DSM 3747: heterologous expression, purification and characterisation. *J. Biotechnol. 80*, 217−230.
22. Waniek, T. (2000) Untersuchungen zur Substratspezifität und Enantioselektivität mikrobieller Hyantoinasen. Dissertation Universität Stuttgart, Germany.
23. Keil, O., Schneider, M. P., and Rasor, J. P (1995) New hydantoinases from thermophilic microorganisms−synthesis of enantiomerically pure D-amino acids. *Tetrahedron: Asymmetry 6*, 1257−1260.
24. May, O., Siemann, M., Syldatk, C, Niefind, K., and Schomburg, D. (1996) Crystallisation and preliminary X-ray analysis of a hydantoinase from *Arthrobacter aurescens* DSM 3745. *Acta Crystallogr., Sect. D 52*, 1209−1210.
25. Brünger, A. T. (1992) *X-PLOR−A system for X-ray crystallography and NMR*, Yale University Press, New Haven, CT.
26. Tong, L., and Rossmann, M. R. (1997) Rotation function calculations with GLRF program. *Methods Enzymol. 276*, 594−611.
27. Brünger, A. T., Adams, P. D., Clore, G. M., DeLano, W. L., Gros, P., Grosse-Kunstleve, R. W., Jiang, J.-S., Kuszewski, J., Nilges, N., Pannu, N. S., Read, R. J., Rice, L. M., Simonson, T., and Warren, G. L. (1998) Crystallography and NMR system (CNS): A new software system for macromolecular structure determination. *Acta Crystallogr., Sect. D 54*, 905−921.
28. Thompson, J. D., Higgins, D. G., and Gibson, T. J. (1994) CLUSTAL W: improving the sensitivity of progressive multiple sequence alignment through sequence weighting, position-specific gap penalties and weight matrix choice. *Nucleic Acids Res. 22*, 4673−4680.
29. Sali, A., and Blundell, T. L. (1993) Comparative protein modelling by satisfaction of spatial restraints. *J. Mol. Biol. 234*, 779−815.
30. Jones, T. A., Zou, J. Y., Cowan, S. W., and Kjeldgaard, M. (1991) Improved methods for binding protein models in electron density maps and the location of errors in these models. *Acta Crystallogr., Sect. A 47*, 110−119.
31. Laskowski, R. A., MacArthur, M. W., Moss, D. S., and Thornton, J. M. (1993) PROCHECK: A program to check the stereochemical quality of protein structures. *J. Appl. Crystallogr. 26*, 283−291.
32. Kabsch, W., and Sander, C. (1983) Dictionary of protein secondary structure: pattern recognition of hydrogen-bonded and geometrical features. *Biopolymers 22*, 2577−2637.
33. Gasteiger, J., Sadowski, J., Schuur, J., Selzer, P., Steinhauer, L., and Steinhauer, V. (1996) Chemical Information in 3D-Space. *J. Chem. Inf. Comput. Sci. 36*, 1030−1037.
34. Karplus, P. A., Pearson, M. A., and Hausinger, R. P. (1997) 70 years of crystalline urease: what have we learned? *Acc. Chem. Res. 30*, 330−337.
35. Ciurli, S., Benini, S., Rypniewski, W. R., Wilson, K. S., Miletti, S., and Mangani, S. (1999) Structural properties of the nickel ions in urease: novel insights into the catalytic and inhibition mechanisms. *Coord. Chem. Rev. 190−192*, 331−355.
36. May, O., Nguyen, P. T., and Arnold, F. H. (2000) Inverting enantioselectivity by directed evolution of hydantoinase for improved production of L-methionine. *Nat. Biotechnol. 18*, 317−320.
37. Kraulis, P. J. (1991) MOLSCRIPT: A program to produce both detailed and schematic plots of protein structures. *J. Appl. Crystallogr. 24*, 946−950.
38. Merritt, E. A., and Cacon, D. J. (1997) Raster3D: photorealistic molecular graphics. *Methods Enzymol. 277*, 505−524.
39. Westhead, D. R., Slidel, T. W., Flores, T. P., and Thornton, J. M. (1999) Protein structural topology: Automated analysis and diagrammatic representation. *Protein Sci. 8*, 897−904.

BI0157722